

Neutrino Indirect Detection of Neutralino Dark Matter in the CMSSM.

V. Bertin ¹, E. Nezri ^{1 2}, J. Orloff ²

Centre de Physique des Particules de Marseille F-13288 Marseille Cedex 09
 Laboratoire de Physique Corpusculaire de Clermont-Ferrand F-63177 Aubiere Cedex
 email : bertin@cppm.in2p3.fr, nezri@in2p3.fr, orloff@in2p3.fr

January 23, 2020

Abstract

We study potential signals of neutralino dark matter indirect detection by neutrino telescopes in a wide range of CMSSM parameters. We also compare with direct detection potential signals taking into account in both cases present and future experiment sensitivities. Only models with neutralino annihilation into gauge bosons can satisfy cosmological constraints and current neutrino indirect detection sensitivities. For both direct and indirect detection, only next generation experiments will be able to really test this kind of models.

Contents

1	Introduction	1
2	Neutralino in the CMSSM	2
3	Branching ratios in neutralino annihilation	3
4	Neutralino-proton cross section : capture rate and direct detection signals.	6
5	Neutrino indirect detection	7
6	Variations	9
7	Conclusion	12

1 Introduction

Our present understanding of the universe is described in the context of general relativity and cosmology. The densities of its components are related by [1] :

$$\Omega(a) - 1 = \frac{\Omega_{tot} - 1}{1 - \Omega_{tot} + \Omega_\Lambda a^2 + \Omega_{mat} a^{-1} + \Omega_{rel} a^{-2}} , \quad (1)$$

where a is the scale factor. This equation and current experimental results suggest and focus on a flat universe with the following parameters [2] :

cosmological constant : $\Omega_\Lambda = 0.7 \pm 0.1$

matter : $\Omega_{mat} = 0.3 \pm 0.1$

baryonic matter : $\Omega_b = 0.04 \pm 0.01$; including $\Omega_{vis} \lesssim 0.01$

cold dark matter : $\Omega_{DM} = 0.26 \pm 0.1$

relativistic components : $0.01 \lesssim \Omega_{rel} \lesssim 0.05$

neutrinos : $0.01 \lesssim \Omega_\nu \lesssim 0.05$

photons : $\Omega_\gamma = 4.8_{-0.9}^{+1.3} \times 10^{-5}$

Hubble's constant : $h \equiv H_0/100 \text{ km}^{-1} \cdot \text{s}^{-1} \cdot \text{Mpc}^{-1} = 0.72 \pm 0.08$

In the framework of the Minimal SuperSymmetric Model (MSSM) [3, 4, 5, 6, 7], the lightest supersymmetric particle (LSP) is typically the lightest of the neutralinos $\chi_1 (\equiv \chi), \chi_2, \chi_3, \chi_4$, the mass eigenstates of the neutral gauge and Higgs boson superpartners $(\tilde{b}, \tilde{W}^3, \tilde{H}_d^0, \tilde{H}_u^0)$. Assuming R-parity conservation ($R \equiv (-1)^{B+L+2S}$), the neutralino is stable and is typically a good candidate for cold dark matter [8]. In this context, all sparticles produced after the big-bang give a neutralino in their decay chain, leading to a relic bath of χ in the present universe. These neutralinos could be observed via direct detection (χ interaction with a nucleus of a detector), or indirect detection of their annihilation products ($\nu, \gamma, \bar{p}, \bar{D}, e^+$). We will mainly focus in this paper on ν indirect detection. The relic neutralinos are gravitationally captured by massive astrophysical bodies and accumulated at the centre of these objects by successive elastic scatterings on their nuclei. The captured neutralino population annihilates and gives rise to neutrino fluxes which could be detectable in neutrino telescopes like Amanda/Icecube, Antares, Baikal.

2 Neutralino in the CMSSM

In the MSSM, the mass matrix of neutralinos in the basis $(-\tilde{b}, -\tilde{W}^3, \tilde{H}_d^0, \tilde{H}_u^0)$ is

$$M_{\chi_1, \chi_2, \chi_3, \chi_4} = \begin{pmatrix} M_1 & 0 & -m_Z \cos \beta \sin \theta_W & m_Z \sin \beta \sin \theta_W \\ 0 & M_2 & m_Z \cos \beta \cos \theta_W & -m_Z \sin \beta \cos \theta_W \\ -m_Z \cos \beta \sin \theta_W & m_Z \cos \beta \cos \theta_W & 0 & -\mu \\ m_Z \sin \beta \sin \theta_W & -m_Z \sin \beta \cos \theta_W & -\mu & 0 \end{pmatrix} \quad (2)$$

where M_1, M_2 are mass term of $U(1)$ and $SU(2)$ gaugino fields, μ is the higgsino “mass” parameter and $\tan \beta = \langle H_u \rangle / \langle H_d \rangle$ is the ratio of the neutral Higgs vacuum expected values.

The neutralino composition is :

$$\chi = N_1 \tilde{b} + N_2 \tilde{W}^3 + N_3 \tilde{H}_d^0 + N_4 \tilde{H}_u^0 \quad (3)$$

and we define its gaugino fraction as : $g_{frac} = |N_1|^2 + |N_2|^2$.

In this model, the introduction of soft terms in the Lagrangian breaks explicitly supersymmetry, leading to a low energy effective theory with 124 parameters. The MSSM is therefore not very predictive, and a non biased exploration of its parameter space is not possible. As a first step, we will therefore as usual concentrate on gravity-mediated supersymmetry breaking in supergravity [9] inspired models, with Grand Unification of soft terms at $E_{GUT} \sim 2.10^{16}$ GeV parameterized by m_0 (common scalar mass), $m_{1/2}$ (common gaugino mass) and A_0 (common trilinear term). Together with $\tan \beta$ and $sgn(\mu)$, these define a 5 parameters constraint MSSM (CMSSM) or mSugra model. [10, 11, 12] model, from which the 124 parameters can be deduced through renormalization group equations (RGE).

Due to large top Yukawa coupling, renormalization group evolution can drive $m_{H_u}^2|_{Q_{EWSB}}$ and/or $m_{H_d}^2|_{Q_{EWSB}}$ to negative values, such that the electroweak symmetry breaking (EWSB) originates purely in quantum corrections ; which realizes *radiative electroweak symmetry breaking*. Minimization of the scalar potential at the electroweak breaking scale Q_{EWSB} yields the condition :

$$\frac{1}{2} m_Z^2 = \frac{m_{H_d}^2|_{Q_{EWSB}} - m_{H_u}^2|_{Q_{EWSB}} \tan^2 \beta}{\tan^2 \beta - 1} - \mu^2|_{Q_{EWSB}} \underset{\tan \beta \gtrsim 5}{\sim} -m_{H_u}^2|_{Q_{EWSB}} - \mu^2|_{Q_{EWSB}}, \quad (4)$$

where usually $Q_{EWSB} \sim \sqrt{m_{\tilde{t}_1} m_{\tilde{t}_2}}$ [13] to minimize one loop contributions.

Such mSugra models offer the theoretical advantage over generic MSSM models that problems such as Landau poles, charge and color breaking (CCB) minima are partially addressed when dealing with RGE.

In mSugra, there are two kinds of neutralinos [14, 15] :

- almost pure bino-like neutralino :

RGE drive $M_1|_{Q_{EWSB}} \simeq 0.41 M_1|_{GUT} = 0.41 m_{1/2} \ll |\mu|_{Q_{EWSB}}$
and $M_2|_{Q_{EWSB}} \simeq 0.83 M_1|_{GUT} = 0.83 m_{1/2} \ll |\mu|_{Q_{EWSB}}$

- for $m_0 \gtrsim 1000$ GeV, the neutralino can be a bino-higgsino mixture ($\tan \beta \gtrsim 5$) :

The increase of m_0 drives $m_{H_u}^2$ to be less negative so that both $|m_{H_u}^2|$ and $|\mu|$ (via eq. 4) decrease. One can then have $|\mu|_{Q_{EWSB}} \lesssim M_1|_{Q_{EWSB}}$ depending on $m_{1/2}$. When $|\mu|$ is too small, EWSB cannot be achieved.

In addition the very low m_0 region can lead to models with tachyonic sfermions (low $m_{1/2}$) or a slepton LSP.

These two behaviors are shown on figure 1 in the $(m_0, m_{1/2})$ plane. The neutralino mass is $\sim 0.4 m_{1/2}$ but is affected by low μ values at high m_0 .

$A_0=0$; $\tan(\beta)=45$; $\mu > 0$

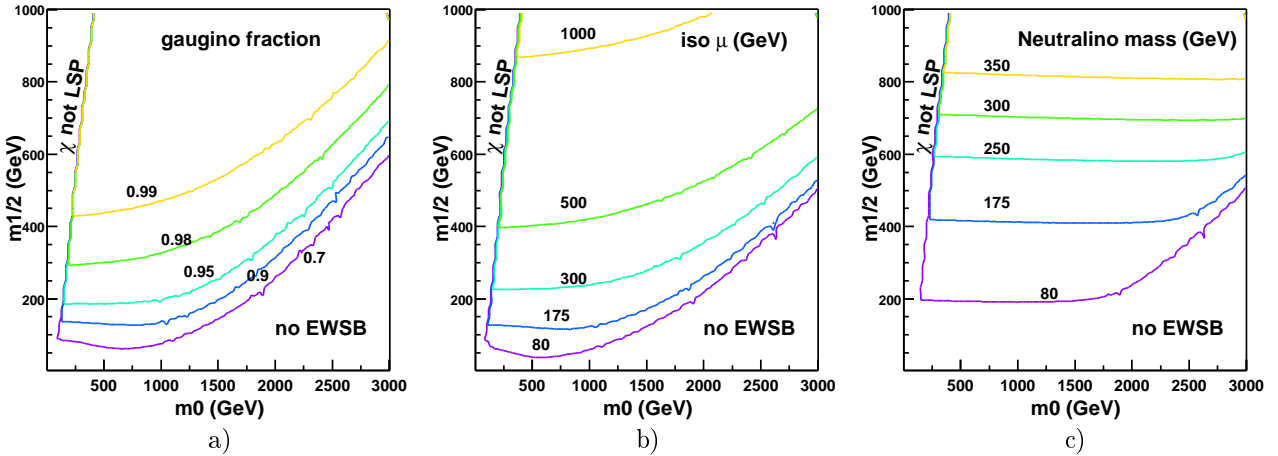


Figure 1: a) Gaugino fraction, b) value of μ and c) neutralino mass in the $(m_0, m_{1/2})$ plane. Region where χ is not the LSP or EWSB is not achieved are also indicated. Our default choice for top mass and the potential minimization scale are : $m_t = 174, 3$ GeV and $Q_{EWSB} = \sqrt{m_{\tilde{t}_1} m_{\tilde{t}_2}}$, except in the last section when these values are specified explicitly.

In this paper, the RGE, SUSY spectrum and potential minimization are derived using the SUSPECT program [16, 17] which includes 2 loops RGE [18], tadpole method to minimize the scalar potential [19] and all radiative corrections in the mass spectrum [20]. The neutralino relic density, including $\chi\chi^+$ and $\chi\chi_2$ coannihilations, and detection signals are calculated by the DarkSUSY (DS) package [21, 22]¹ which correctly implements s-channel poles and thresholds [23]. Our interface (available from nezri@in2p3.fr, submitted for inclusion in DS) shortcuits the DS spectrum recalculation, to comply with the SUSPECT spectra which have been checked [24] against SOFTSUSY [25].

3 Branching ratios in neutralino annihilation

The leading processes in neutralino annihilation are shown in figure 2, where the last two processes are proportional to the higgsino/wino fraction of χ and $\chi_i^{(+)}$.

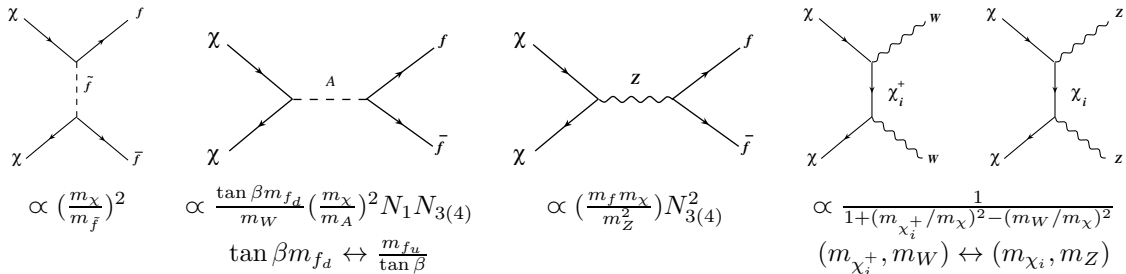


Figure 2: Leading channels in neutralino annihilation, with their parametric dependance of their amplitude, N_i being defined in equation 3 [8].

In mSugra models, one can typically distinguish different regions of annihilation branching ratios in the $(m_0, m_{1/2})$ plane, for almost any values of $\tan \beta (\geq 5)$ (see figure 3).

Above top thresholds : $m_\chi \gtrsim m_{top} \Leftrightarrow m_{1/2} \gtrsim 400$ GeV or slightly higher in the mixed higgsino region.

Region I : low m_0 ($< 500 - 1000$ GeV), the neutralino is almost purely bino like. Despite a very low higgsino fraction of χ , the Z exchange amplitude, being proportional to the sfermion mass, is significant in

¹These calculations use a neutralino local density $\rho_\chi = 0.3$ GeV/cm³ and a Maxwellian velocity distribution with $v_0 = 220$ km · s⁻¹

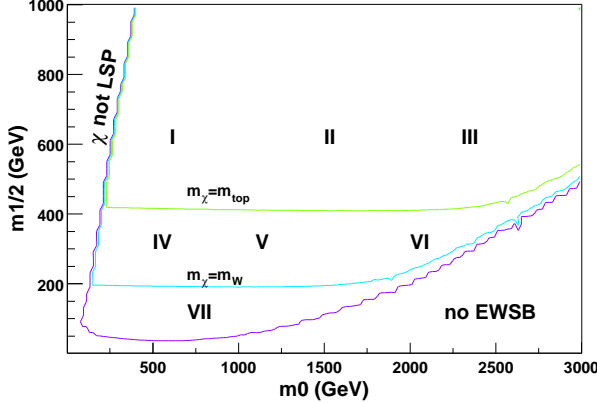


Figure 3: Typical regions of neutralino annihilation.

the top channel $\chi\chi \xrightarrow{Z} t\bar{t} \propto (m_t m_\chi / m_Z^2)^2 N_{3(4)}^2$. The leading processes are $\chi\chi \xrightarrow{\tilde{t}} t\bar{t}$ and $\chi\chi \xrightarrow{Z} t\bar{t}$, which have an opposite sign. This cancellation makes $\chi\chi \xrightarrow{A} b\bar{b}$ become the dominant process. Its amplitude $\propto \frac{\tan\beta m_b}{m_W} (\frac{m_\chi}{m_A})^2 N_1 N_{3(4)}$ is strongly enhanced for high $\tan\beta$, both from the explicit dependence, and because m_A decreases when $\tan\beta$ increases. So in the region I, the total annihilation cross section $\sigma_{\chi-\chi}^A$ is important for high values of $\tan\beta$.

Region II : when m_0 increases ($< 1500 - 2000$ GeV), m_A increases and, for intermediate $\tan\beta$ values, the $\chi\chi \xrightarrow{A} b\bar{b}$ amplitude decreases. Since sfermion masses also increase, the $\chi\chi \xrightarrow{\tilde{t}} t\bar{t}$ channel no longer cancels $\chi\chi \xrightarrow{Z} t\bar{t}$, which becomes the dominant process. However, for high $\tan\beta$, $\chi\chi \xrightarrow{A} b\bar{b}$ is enhanced and stays dominant. Globally, since all scalar masses have been increased by m_0 , and the higgsino fraction is still small, the neutralino annihilation cross section is smaller than in region I.

Region III : increasing further m_0 ($> 2000 - 2500$ GeV), for any value of $\tan\beta$, one finally approaches the mixed higgsino-bino region. The $\chi\chi \xrightarrow{Z} t\bar{t}$ channel $\propto (\frac{m_t m_\chi}{m_Z^2})^2 N_{3(4)}^2$ then dominates all other processes, which are suppressed by the increase of scalar masses. So we are left with a $t\bar{t}$ region parallel to the highest higgsino fraction isocurves. The m_0 value separating this region from the previous $\chi\chi \xrightarrow{A} b\bar{b}$ region depends on $\tan\beta$. All in all, the neutralino annihilation is strongly enhanced by Z exchange near the no-EWSB boundary.

Between top and W/Z thresholds :

Region IV : since $m_\chi < m_{top}$, the neutralino annihilates almost only into $b\bar{b}$. Even if some $\chi\chi \xrightarrow{\tilde{b}} b\bar{b}$ occurs, the $\chi\chi \xrightarrow{A} b\bar{b}$ amplitude is dominant.

Region V : increasing m_0 (and m_A), $\chi\chi \xrightarrow{A} b\bar{b}$ remains dominant and this process is still quite efficient for high values of $\tan\beta$. For intermediate values of $\tan\beta$, $\chi\chi \xrightarrow{A} b\bar{b}$ and $\chi\chi \xrightarrow{Z} b\bar{b}$ both occur but their amplitudes are small and the total annihilation is not efficient.

Region VI : increasing further m_0 disfavours scalar exchange, but even small, the higgsino fraction allows $\chi\chi \xrightarrow{\chi_i^+} W^+ W^-$ and $\chi\chi \xrightarrow{\chi_i} ZZ$ to dominate and enhance the total annihilation cross section $\sigma_{\chi-\chi}^A$. Again, the m_0 values delimiting the boundary with region V depend on $\tan\beta$ (via m_A).

Below W/Z thresholds :

Region VII : the dominant process is $\chi\chi \rightarrow b\bar{b}$ via A and/or Z exchange, depending on m_0 , $\tan\beta$ and the higgsino fraction.

This analysis is illustrated on figures 4 and 13, showing the four most important branching ratios for $\tan\beta = 45$ and 10 (the omitted process $\chi\chi \xrightarrow{A} \tau\bar{\tau}$ behaves as $\chi\chi \xrightarrow{A} b\bar{b}$ but with a smaller amplitude due to the m_τ/m_b ratio).

It offers a qualitative understanding of the relic density picture (figure 5). The annihilation is efficient for low values of m_0 (depending on $\tan\beta$) and for a mixed neutralino along the no-EWSB boundary. This gives the “V” (or “U”) shape of the relic density profile for large (or small) $\tan\beta$. According to the current cosmological parameter values, we take the neutralino as an interesting cold dark matter candidate if $0.025 < \Omega h^2 < 0.3$. Figure 5 also shows the region in the $(m_0, m_{1/2})$ plane excluded by the experimental

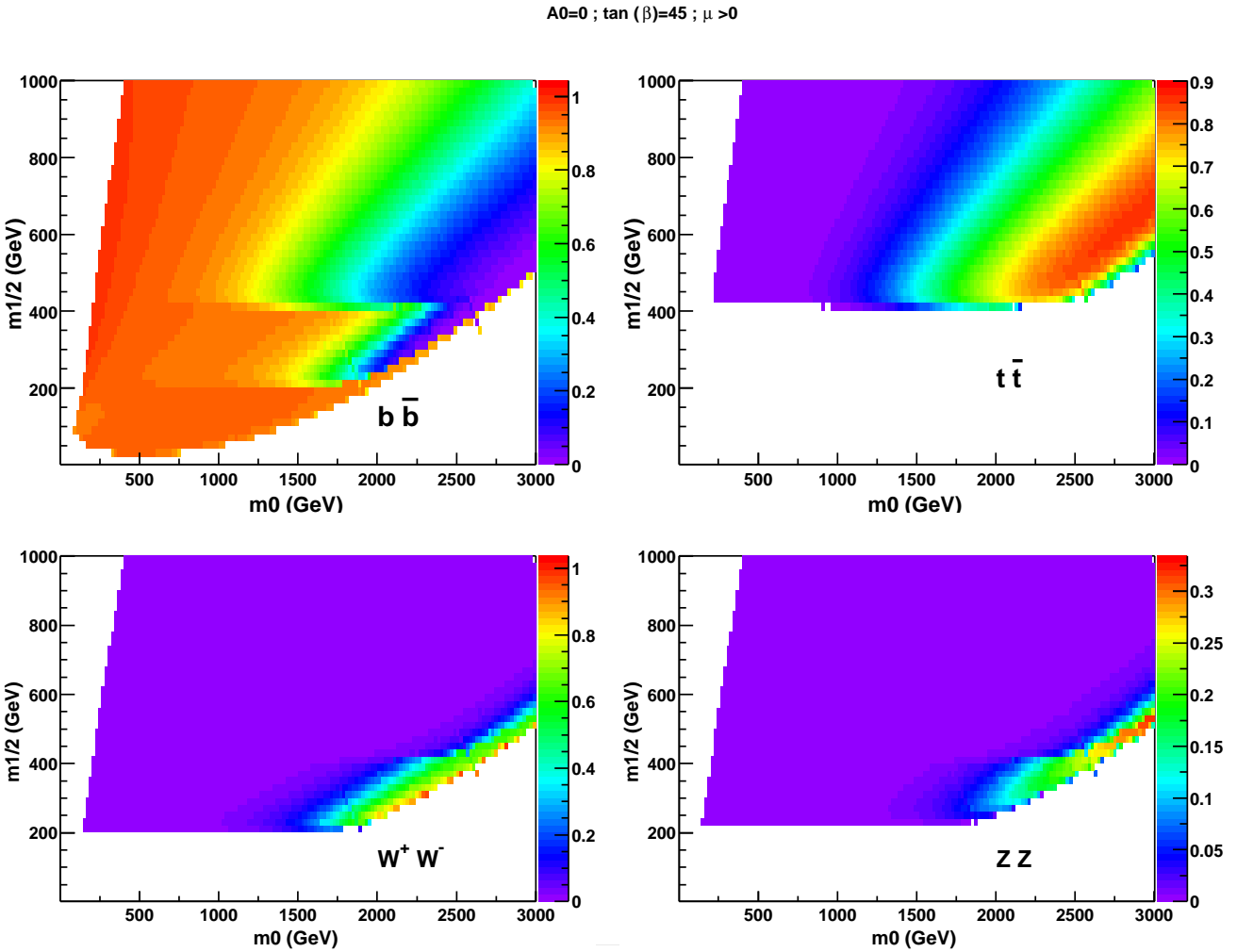


Figure 4: Dominant branching ratios of the neutralino annihilation in the $(m_0, m_{1/2})$ plane

constraints from the Particle Data Group 2000 [26] implemented in DarkSusy, that we have updated with : $m_{\chi_1^+} > 104$ GeV ; $m_{\tilde{f}} > 100$ GeV for $\tilde{f} = \tilde{t}_1, \tilde{b}_1, \tilde{t}^\pm, \tilde{\nu}$, $m_{\tilde{g}} > 300$ GeV ; $m_{\tilde{q}_{1,2}} > 260$ GeV for $\tilde{q} = \tilde{u}, \tilde{d}, \tilde{s}, \tilde{c}$ and $-6 \cdot 10^{-10} < a_\mu(\text{SUSY}) < 58 \cdot 10^{-10}$ [27].

As noted in previous studies [28, 17], the muon anomalous moment and $b \rightarrow s\gamma$ strongly favours $\mu > 0$, to which we restrict in what follows. In figure 5, the grey tail at large m_0 is excluded by the chargino bound ; it directly bites into the region relevant for neutrino indirect detection. Less relevant is the exclusion of small m_0 and $m_{1/2}$ values, which comes both from the Higgs mass limit and the $b \rightarrow s\gamma$ branching ratio, as calculated by default in DS. The range $BR(b \rightarrow s\gamma) = 1 \rightarrow 4 \times 10^{-4}$ chosen by default in DarkSusy may seem too low in view of latest CLEO and Belle measurements [26]. However the leading order calculation [29] implemented underestimates the SM value to 2.4×10^{-4} , while next to leading order corrections give 3.6×10^{-4} [30] so that this range should roughly correspond to $2.2 \rightarrow 5.2 \times 10^{-4}$, excluding a bit more than the range $2 \rightarrow 5 \times 10^{-4}$ chosen for instance in [17]. We have checked that replacing the implemented Higgs limit [31] by an aggressive version of the latest limit [32] ($m_h > 114$ GeV for all $\sin(\beta - \alpha)$) only excludes a few more points around $(m_0 = 1000, m_{1/2} = 150)$ where neutrino fluxes are beyond reach.

In mSugra, $\chi\chi^+$ and $\chi\chi_2$ coannihilations (included in DS) happen only in the mixed neutralino region, decreasing further the relic density. $\chi\tilde{\tau}$ coannihilation happens for low values of $\tan\beta$, for which there is no mixed region. $\chi\tilde{t}$ coannihilation [33, 17, 34] happens for high values of A_0 . In both cases, sfermion coannihilations (missing in DS) are relevant to lower the relic density in regions of large m_χ , which we will see are beyond reach of indirect detection. We therefore do not expect their proper inclusion to change our conclusions.

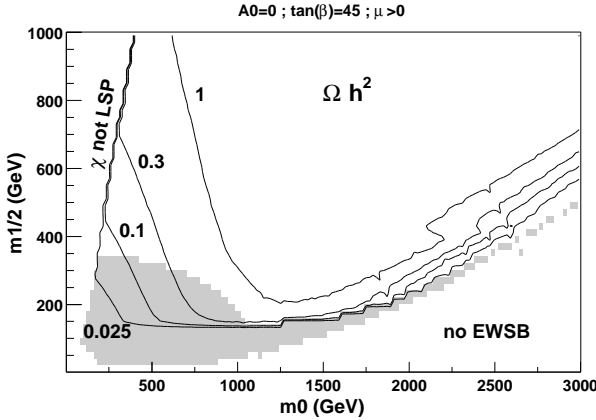


Figure 5: Neutralino relic density in the $(m_0, m_{1/2})$ plane. Grey area indicates the excluded models by current accelerators constraints as discussed in the text.

4 Neutralino-proton cross section : capture rate and direct detection signals.

Capture :

If present in the halo, relic neutralinos must accumulate in astrophysical bodies (of mass M_b) like the Sun or the Earth. The capture rate C depends on the neutralino-quark elastic cross section : $\sigma_{\chi-q}$. Neutralinos being Majorana particles, their vectorial interaction vanishes and the allowed interactions are scalar (via $\chi q \xrightarrow{H,h} \chi q$ in t channel and $\chi q \xrightarrow{\bar{q}} \chi q$ in s channel) and axial (via $\chi q \xrightarrow{Z} \chi q$ in t channel and $\chi q \xrightarrow{\bar{q}} \chi q$ in s channel). Depending on the spin content of the nuclei N present in the body, scalar and/or axial interactions are involved. Roughly $C \sim \frac{\rho_\chi}{v_\chi} \sum_N M_b f_N \frac{\sigma_N}{m_\chi m_N} < v_{esc}^2 >_N F(v_\chi, v_{esc}, m_\chi, m_N)$, where ρ_χ, v_χ are the local neutralino density and velocity, f_N is the density of nucleus N in the body, σ_N the nucleus-neutralino elastic cross section, v_{esc} the escape velocity and F a suppression factor depending on masses and velocity mismatching. As $M_\odot \gg M_\oplus$, the neutralino capture is much more efficient in the Sun than in the Earth and is maximized for $m_\chi \sim m_N$ as $\frac{\sigma_N}{m_\chi m_N} \sim \frac{m_{red}^2}{m_\chi m_N} = \frac{m_\chi m_N}{(m_\chi + m_N)^2}$.

For the Earth, scalar interactions dominate. By increasing m_0 from its low value region, sfermions and H exchanges first decrease, and the cross-section rises again when approaching the mixed higgsino region (see figure 6a). The capture rate is resonant for $m_\chi \sim 56$ GeV around the iron mass.

For the Sun, the spin of hydrogen allows for axial interaction, which is higher due to the Z coupling. The latter depends strongly on the neutralino higgsino fraction and is independent of $\tan\beta$, so the cross-section follows the higgsino fraction isocurves as can be seen by comparing figure 6b and 1.

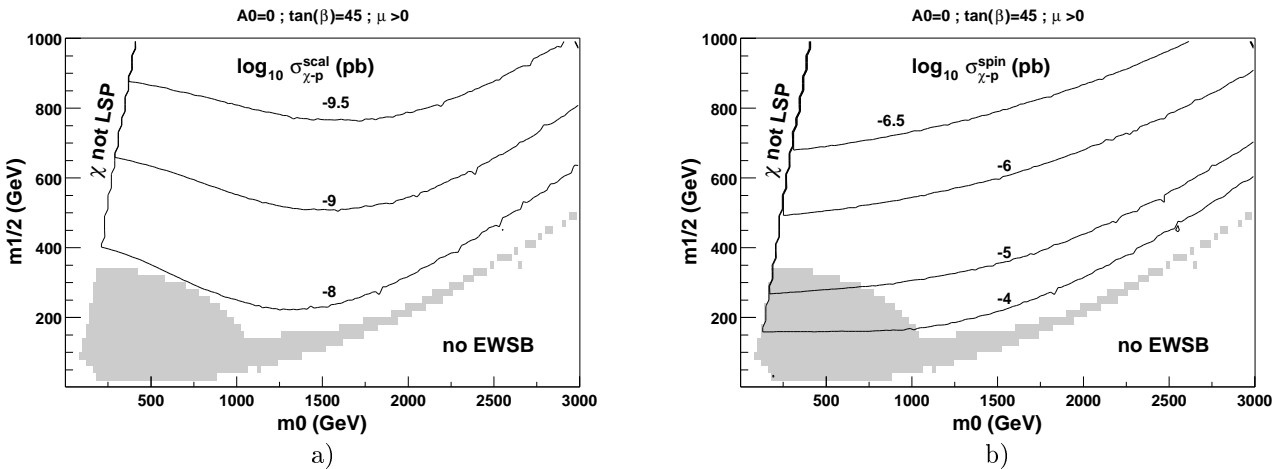


Figure 6: Scalar (a) and axial (b) cross sections for neutralino scattering on proton in pb.

To summarize, due to the large solar mass and the spin dependent neutralino-quark cross section, the storage of neutralinos is much more efficient in the Sun than in the Earth.

Direct detection :

The elastic cross section of neutralino on a nucleus also depends on $\sigma_{\chi-q}$, the nucleus mass number A and its spin content. Depending on the chosen nuclei target, current and future direct detection experiments are sensitive to the scalar coupling (CDMS (Ge) [35], Edelweiss (Ge) [36], Zeplin (Xe) [37]) or to the axial coupling (MACHe3 (${}^3\text{He}$) [38]. Comparison between experiment sensitivities and a set of mSugra models are shown on figure 9.

5 Neutrino indirect detection

As $\chi\chi \rightarrow \nu\bar{\nu}$ is strongly suppressed by the tiny neutrino mass, neutrino fluxes come from decays of primary annihilation products, with a mean energy spectrum $E_\nu \sim \frac{m_\chi}{2}$ to $\frac{m_\chi}{3}$. The most energetic spectra, called “hard” come from neutralino annihilations into WW , ZZ and the low energetic, “soft”, ones comes from $b\bar{b}$ [21]. Muon neutrinos give rise to muon fluxes by charged-current interactions in the Earth. As both the ν charged-current cross section and the produced muon range are proportional to E_ν , high energy neutrinos are easier to detect. Considering that the population of captured neutralinos has a velocity below the escape velocity, and therefore neglecting evaporation, the number N_χ of neutralinos in the centre of a massive astrophysical object depends on the balance between capture and annihilation rates : $\dot{N}_\chi = C - C_A N_\chi^2$, where C_A is the total annihilation cross section times relative velocity per volume. The annihilation rate at a given time t is then :

$$\Gamma_A = \frac{1}{2} C_A N_\chi^2 = \frac{C}{2} \tanh^2 \sqrt{CC_A} t \quad (5)$$

with $\Gamma_A \approx \frac{C}{2} = \text{cste}$ when the neutralino population has reached equilibrium, and $\Gamma_A \approx \frac{1}{2} C^2 C_A t^2$ in the initial collection period (Earth case).

So, when accretion is efficient, the annihilation rate does not depend on annihilation processes, but follows the capture rate C and thus the neutralino-quark elastic cross section.

For the Sun, neutralinos are not in equilibrium in the whole $(m_0, m_{1/2})$ plane studied. This result is different

$A=0$; $\tan(\beta)=45$; $\mu>0$

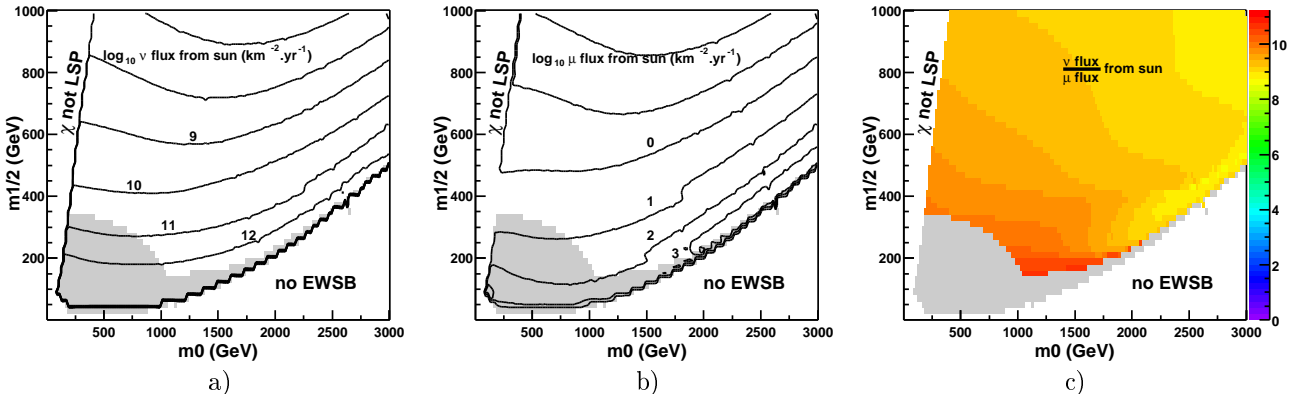


Figure 7: ν fluxes from the Sun (a), the corresponding μ fluxes above 5 GeV (b) and their ratio (c).

from [28] where the calculation is based on Neutdriver [8]. In our calculation we find that the annihilation is on average less efficient, and equilibrium more difficult to reach. For high m_0 values, equilibrium is reached and $\nu(\mu)$ fluxes follow essentially the higgsino fraction 1a and the spin dependent $\sigma_{\chi-p}^{\text{spin}}$ isocurves 6. For low m_0 , the equilibrium fluxes would drop with m_0 and C , but the smaller capture rate hinders equilibrium (eg $\sqrt{CC_A} t_\odot \sim 1$ for $m_0 = 500$, $m_{1/2} = 800$) and the annihilation rate feels the increasing annihilation cross-section. This effect is stronger for high $m_{1/2}$ values where the neutralinos are heavier and more bino-like, and where capture is smaller. This effect is also larger when $\tan\beta$ (and thus $\sigma_{\chi-\chi}^A$) is low, because neutralinos are less in equilibrium, so that $\sigma_{\chi-\chi}^A$ evolution is more felt in $\nu(\mu)$ fluxes (e.g. W and top thresholds appear more clearly).

For the Earth, neutralinos are not in equilibrium. Neutrino fluxes depend on C^2 and annihilation, giving an enhancement in the low and high m_0 regions where fluxes are boosted by annihilation (see figure 6 and

$A_0=0$; $\tan(\beta)=45$; $\mu>0$

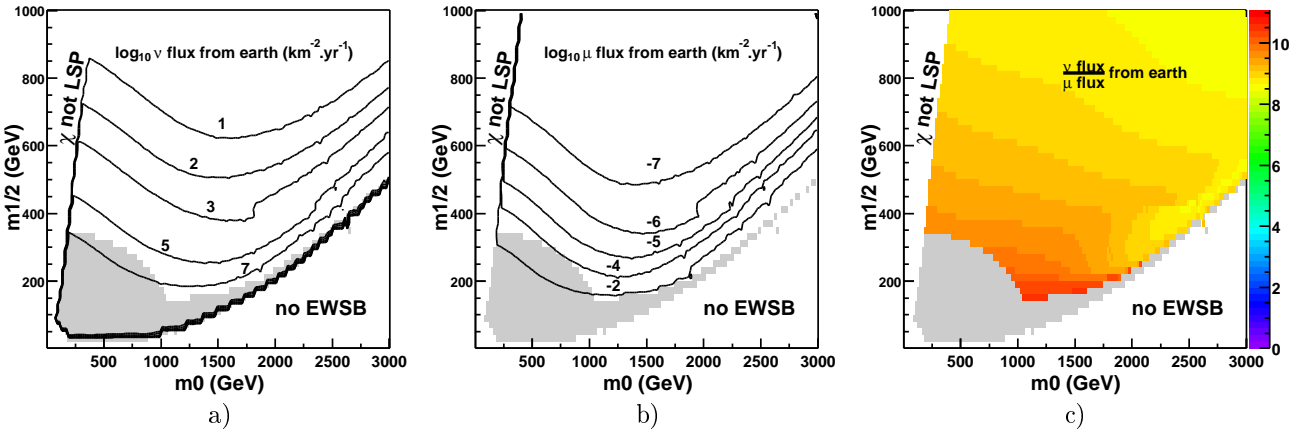


Figure 8: ν fluxes from the Earth (a), the corresponding μ fluxes above 5 GeV (b) and their ratio (c).

8). Since $M_{\oplus} < M_{\odot}$ and $\sigma_{\chi-p}^{scal} < \sigma_{\chi-p}^{spin}$, the capture rate and ν fluxes from the Earth are much smaller than from the Sun.

Comparing ν fluxes and μ fluxes, the $\nu \rightarrow \mu$ conversion factor increases with $m_{1/2}$ due to the increase of m_{χ} leading to more energetic neutrinos. This ratio also follows the annihilation final state regions described above. Indeed, spectra from WW , ZZ and to a lesser extent $t\bar{t}$ are more energetic than $b\bar{b}$ spectra, so neutrino conversion into muon is more efficient in the mixed bino-higgsino region above W and top thresholds (see figure 7 and 8).

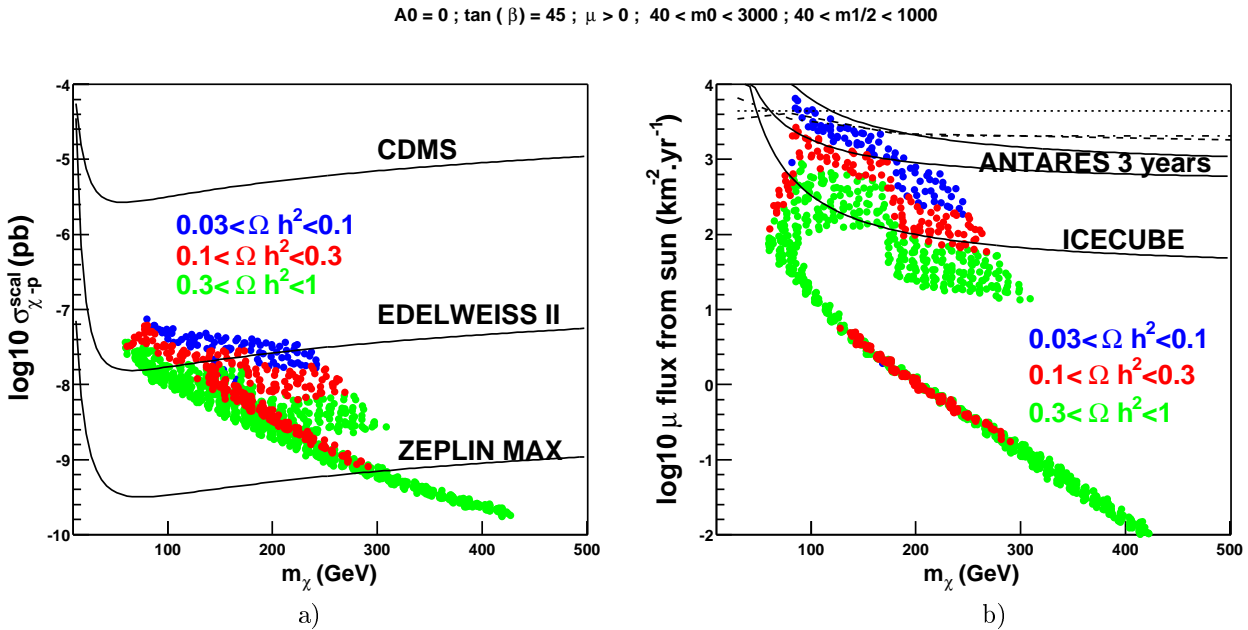


Figure 9: a) Direct detection experiment sensitivities and a set of models in the $(\sigma_{\chi-p}^{scal}, m_{\chi})$ plane. The excluded models by current accelerators constraints are not displayed. b) Indirect detection experiment sensitivities in the $(\mu$ flux $_{\odot}$, m_{χ}) plane with 5 GeV threshold of the same sample as a). Dotted, dash-dotted and dashed curves are respectively the Macro, Baksan and Super-Kamiokande upper limits. Solid lines indicate the future Antares and Icecube sensitivities.

Comparison with indirect detection experiment sensitivities : Muon fluxes coming from neutralinos annihilation in the Sun are shown in figure 9. MSugra models predicting a good relic density of neutralinos give neutrino/muon fluxes which can be as high the current experimental limits(Baksan [39], Macro [40], Super

Kamiokande [41]). The 0.1 km^2 Antares detector will explore further the interesting parameter space [42]. Next generation neutrinos telescopes (Icecube, Antares km^3) will be much more efficient to test such models, eg Icecube expected sensitivity $\sim 10^2 \mu \text{ km}^2 \cdot \text{yr}^{-1}$ from the Sun [43].

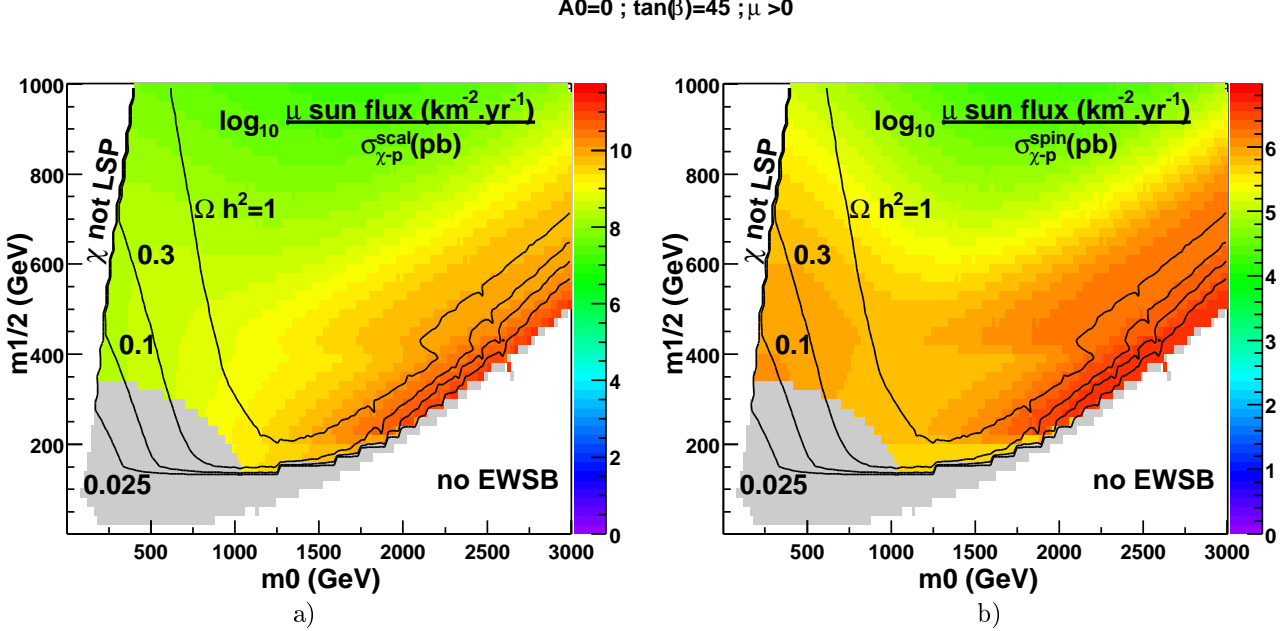


Figure 10: Comparison between μ fluxes from the Sun and neutralino-proton cross sections : a) scalar, b) spin dependent

Indirect vs Direct detection : a high neutralino-proton cross section is efficient to both direct and indirect (via capture) detection. The large m_0 mixed higgsino-bino region pointed out in [15, 28] favours both direct and indirect detection due to the enhancement of $\sigma_{\chi-p}$ and $\sigma_{\chi-\chi}^A$. Both enter in the indirect detection which is moreover favoured by the production of more energetic neutrinos in WW , ZZ , $t\bar{t}$ decays leading to better conversion into muons (figure 10). This mixed region, which has a good relic density, is very attractive for neutrino indirect detection signal.

However, no current experiment is able to really test such models. Figure 11 shows the region of the $(m_0, m_{1/2})$ plane which can be explored by future direct detection experiments and neutrino telescopes.

6 Variations

In this section, we discuss the robustness of the indirect detection picture described above, with respect to variations of 1) mSugra input parameters like A_0 or $\tan\beta$,
2) experimental uncertainties on the top quark mass and
3) theoretical uncertainties on the scale of electroweak symmetry breaking Q_{EWSB}

A_0 : Varying A_0 away from 0 does not change too much the analysis above. Annihilation branching ratio regions, as well as the no-EWSB boundary and slope can be slightly displaced. For moderate $\tan\beta \sim 20$, quite large and negative values of A_0 (eg -800 GeV) can enhance $\tau^+\tau^-$ channel annihilation along the $\tilde{\tau}$ LSP region (*i.e.* low m_0) due to splitting in the \tilde{t} mass matrix. For such values, the $\tilde{\tau}\chi$ coannihilation [44] could also affect the relic density, but in this region, neutrino fluxes are too small to be detected anyway (see figure 12). The same happens with the $t\bar{t}$ channel for $400 < m_{1/2} < 600$ and $m_0 < 700$ ($\sim |A_0|$). The $\tilde{t}\chi$ [33, 17, 34] coannihilation can also happen for $A_0 \sim -2000 \text{ GeV}$, but the usual cosmologically interesting region is reduced (due to the negative squared mass arising in sfermion matrices at low m_0 and because the mixed region is pushed to higher values of m_0). In addition, this coannihilation region produces neutrino fluxes from the Sun around $10^{-1} \mu \text{ km}^{-2} \cdot \text{yr}^{-1}$, too low to be detected. In view of latest results on cosmological parameters, figure 12a shows models with $0.03 < \Omega h^2 < 0.3$ in the $(m_0, m_{1/2})$ plane for different values of A_0 , as well as models giving μ fluxes from the Sun $> 10^2$ (b) and $10^3 \mu \text{ km}^{-2} \cdot \text{yr}^{-1}$ (c). Last models are confined in the mixed higgsino-bino region. In addition, only those models with $m_W < m_\chi < m_t$ giving a hard spectrum of neutrinos via $\chi\chi \xrightarrow{\chi_i^+} W^+W^-$ and $\chi\chi \xrightarrow{\chi_i} ZZ$ can simultaneously satisfy $0.1 < \Omega h^2 < 0.3$,

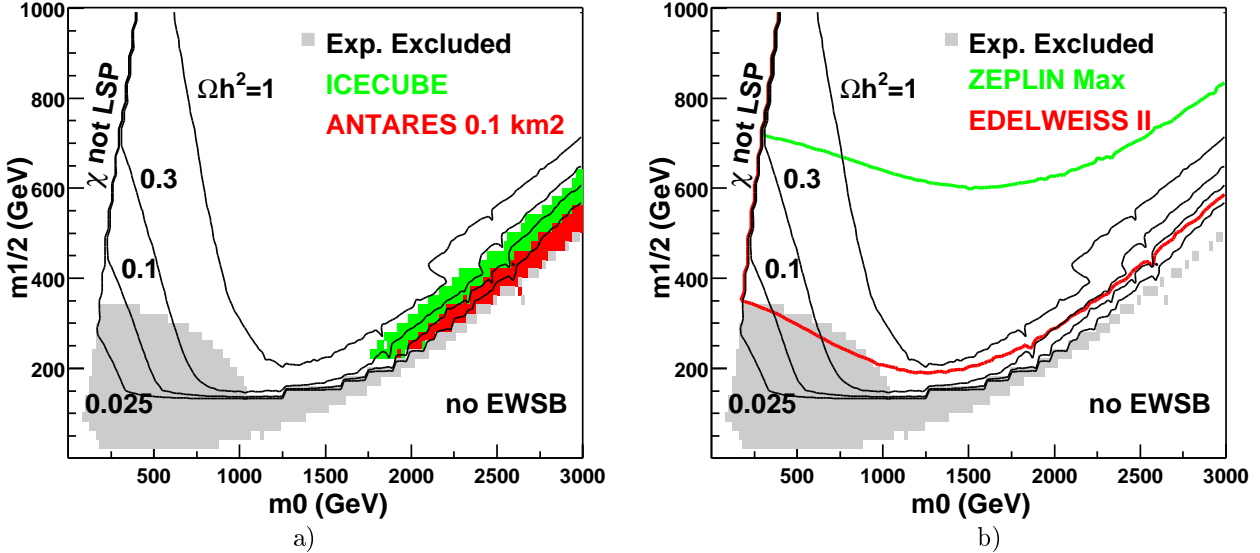


Figure 11: a) ν telescopes sensitivities on μ fluxes from the Sun and b) direct detection experiments sensitivities in the $(m_0, m_{1/2})$ plane.

while yielding a high muon flux.

$\tan \beta$: the branching ratio picture does not qualitatively change for different values of $\tan \beta$. Low values of $\tan \beta$ can add a $\chi\chi \rightarrow t\bar{t}$ region for low m_0 and open a $\tilde{\tau}\chi$ coannihilation [44] region along the $\tilde{\tau}$ LSP region, but μ fluxes are small and such values of $\tan \beta$ reduce the mixed neutralino region which is the most interesting for indirect detection. As discussed previously, the boundaries of branching ratio regions move with $\tan \beta$ (compare figure 13 and 4). When $\tan \beta$ grows, the cosmologically motivated region is wider due to the annihilation enhancement via A exchange (in regions I/II and IV/V). Applying the conservative cut $0.03 < \Omega h^2 < 0.3$, all values of $\tan \beta$ provide interesting models for neutrino indirect detection (see figure 14). For too large values of $\tan \beta$, the bb region is extended and leads to soft neutrino spectra. In this case it becomes more difficult to conciliate a tighter limit on the relic density with current experimental sensitivities. Values of $\tan \beta \sim 10 \rightarrow 35$ give more models satisfying both relic density $0.1 < \Omega h^2 < 0.3$ and high fluxes.

EWSB scale : Q_{EWSB} is the scale at which the running of the soft SUSY breaking terms is frozen and the minimization of the scalar potential is achieved. When the full potential is minimized within a multi-scale RG treatment, Q_{EWSB} should not affect physics. However, the one-loop single scale effective potential does depend on Q_{EWSB} , and the tree-level relations (equation 4) only hold in terms of running parameters at Q_{EWSB} , if Q_{EWSB} is chosen $\sim \sqrt{m_{\tilde{t}_1} m_{\tilde{t}_2}}$ [13] the potential can be minimized perturbatively. Varying Q_{EWSB} away from this value is therefore not physical, but gives a hint on the theoretical uncertainties associated with a single scale RG and potential minimization approach. When Q_{EWSB} is lowered, the RG running drives μ to smaller values. This leads to a wider region of the $(m_0, m_{1/2})$ plane where EWSB cannot be achieved. In the remaining allowed region, the lower values of μ slightly increase the higgsino fraction of the neutralino and the annihilation cross-section giving more cosmologically acceptable models. Figure 15 and 16 shows the relic density and μ fluxes from the Sun and the Earth in the $(m_0, m_{1/2})$ plane for $Q_{EWSB} = \frac{1}{2}$ and $\frac{1}{5}\sqrt{m_{\tilde{t}_1} m_{\tilde{t}_2}}$. For $Q_{EWSB} = \frac{1}{5}\sqrt{m_{\tilde{t}_1} m_{\tilde{t}_2}}$ the annihilation pole of $\chi\chi \xrightarrow{A} b\bar{b}$ in s channel for $m_A \simeq 2m_\chi$ effects is seen which usually appears for higher values of $\tan \beta$. This clearly confirms the strong influence of annihilation processes on $\nu(\mu)$ fluxes coming from the Earth away from equilibrium (figure 16). The higher higgsino fraction also enhances the elastic cross section $\sigma_{\chi-q}$, but the stronger annihilation leads to less models which are both interesting from the cosmological point of view and in terms of Sun muon fluxes (figures 15 and 19). As before, muons fluxes from the Earth are much too weak to be detected. Increasing Q_{EWSB} drives to the opposite effect : higher values of $|\mu|$ and reduced cosmological favoured region.

Top mass : the experimental value is $m_t = 174.3 \pm 5.1$ GeV [26]. Our default choice up to know has been to take the central value. However lowering m_t means that we lower the top Yukawa coupling Y_t so that the RG decreasing of m_H^2 is less efficient and the region where EWSB does not occur is wider (see

$$\tan(\beta) = 35 ; \mu > 0$$

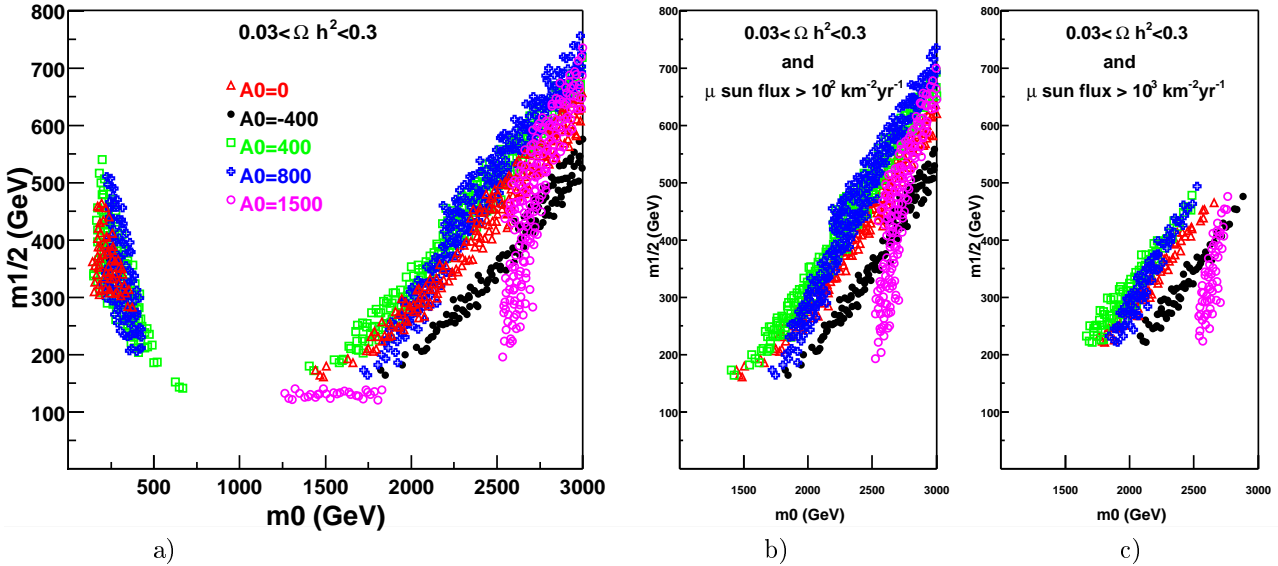


Figure 12: a) Cosmologically favoured models for different values of A_0 in the $(m_0, m_{1/2})$ plane. b) same with μ flux from the Sun $> 10^2 \text{ km}^{-2} \cdot \text{yr}^{-1}$. c) same as a) with μ flux from the Sun $> 10^3 \text{ km}^{-2} \cdot \text{yr}^{-1}$.

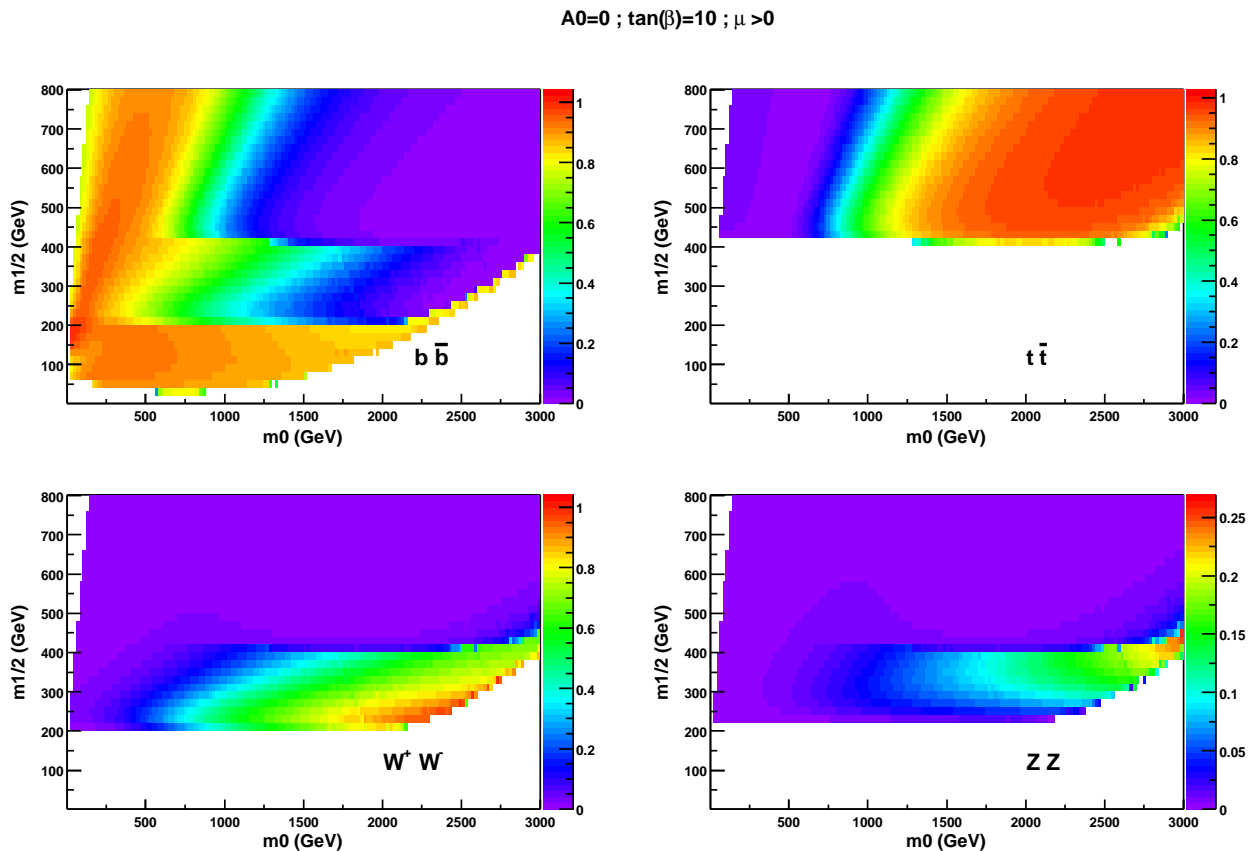


Figure 13: Branching ratio of neutralino annihilation in $(m_0, m_{1/2})$ plane (same as figure 4 for $\tan \beta = 10$).

$$A_0=0 ; \mu >0$$

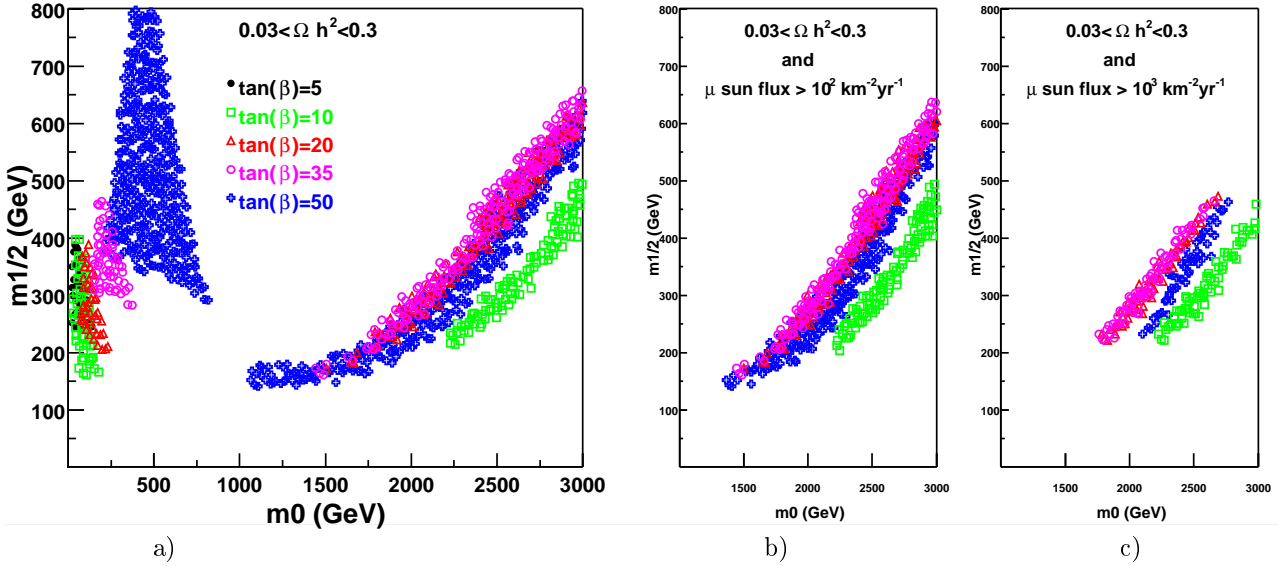


Figure 14: a) Cosmologically favoured models for different values of $\tan\beta$ in the $(m_0, m_{1/2})$ plane. b) same with μ flux from the Sun $> 10^2 \text{ km}^{-2} \cdot \text{yr}^{-1}$. c) same as a) with μ flux from the Sun $> 10^3 \text{ km}^{-2} \cdot \text{yr}^{-1}$.

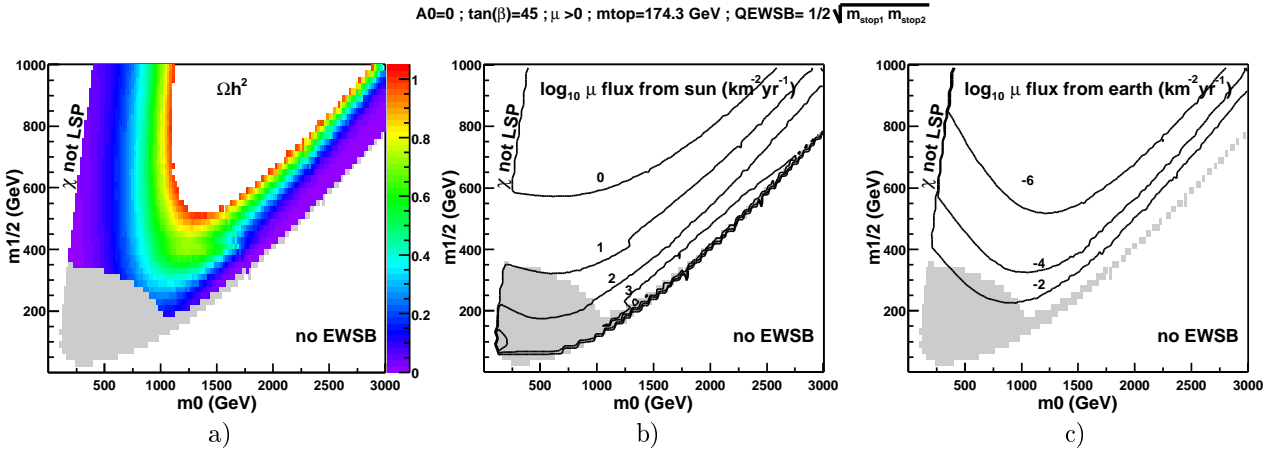


Figure 15: a) Relic density, μ fluxes from the Sun (b) and the Earth (c) in the $(m_0, m_{1/2})$ plane for $Q_{EWSB} = \frac{1}{2}\sqrt{m_{\tilde{t}_1}m_{\tilde{t}_2}}$ and $m_t = 174.3 \text{ GeV}$.

eq.4, figure 17 and 18). Nevertheless the mixed higgsino region is larger favouring annihilation and capture, but there are no additional models satysfying both cosmology and ν/μ fluxes are favoured (figure 17, 18 and 19). Increasing the top mass lead to the opposite effect, which is less interesting for our study.

It should also be noticed that in Q_{EWSB} and/or m_t variation region with heavier neutralino are cosmologically allowed.

7 Conclusion

In this paper, we have analysed, within the framework of the constrained Minimal Supersymmetric Standard Model (a.k.a. mSugra), the possible indirect detection of neutralino dark matter through the neutrinos produced by its annihilation in the Earth and the Sun. In particular, we have presented an original study of the relative weight of various annihilation channels crucial to indirect detection. Fixing the halo dark matter density to $\rho_\chi = 0.3 \text{ GeV}/\text{cm}^3$ and allowing for the widest range of cosmological relic density $0.03 < \Omega h^2 < 0.3$,

A0=0 ; $\tan(\beta)=45$; $\mu > 0$; $m_{top}=174.3$ GeV ; $QEWSB=1/5\sqrt{m_{stop1}m_{stop2}}$

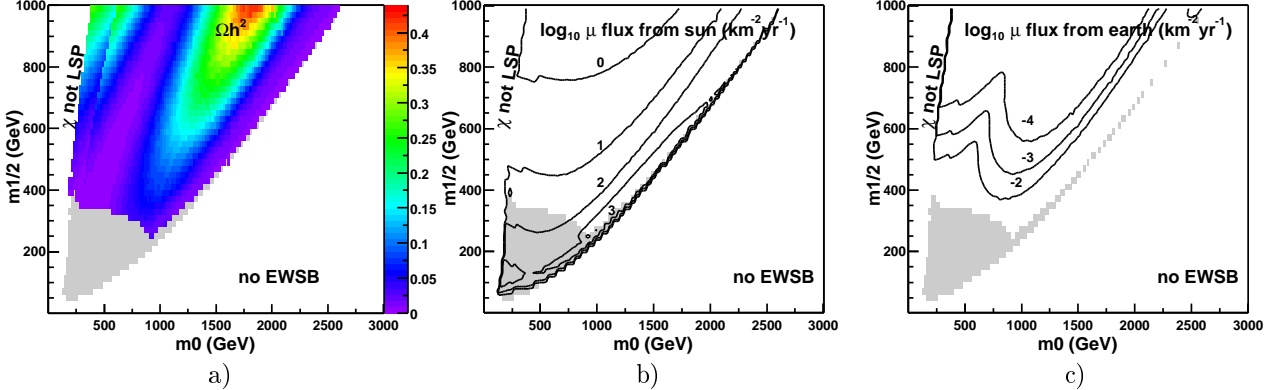


Figure 16: a) Relic density, μ fluxes from the Sun (b) and the Earth (c) in the $(m_0, m_{1/2})$ plane for $Q_{EWSB} = \frac{1}{5}\sqrt{m_{\tilde{t}_1}m_{\tilde{t}_2}}$ and $m_t = 174.3$ GeV.

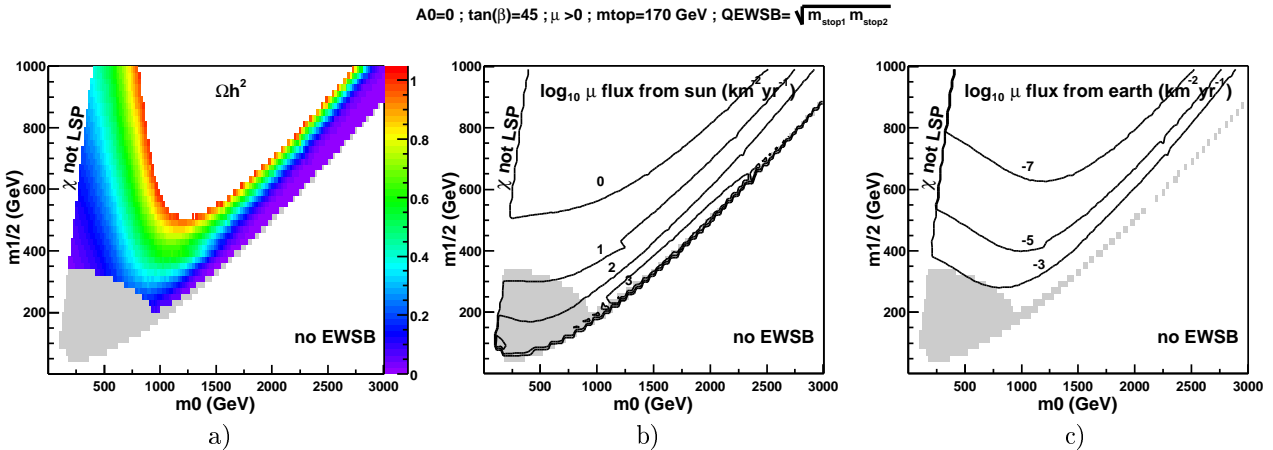


Figure 17: a) Relic density, μ fluxes from the Sun (b) and the Earth (c) in the $(m_0, m_{1/2})$ plane for $Q_{EWSB} = \sqrt{m_{\tilde{t}_1}m_{\tilde{t}_2}}$ and $m_t = 170$ GeV.

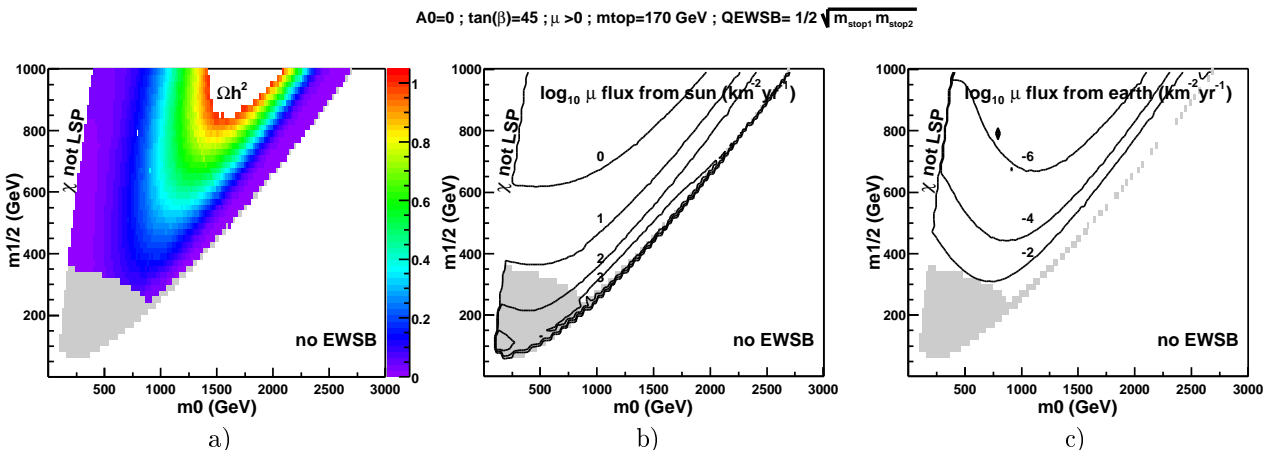


Figure 18: a) Relic density, μ fluxes from the Sun (b) and the Earth (c) in the $(m_0, m_{1/2})$ plane for $Q_{EWSB} = \frac{1}{2}\sqrt{m_{\tilde{t}_1}m_{\tilde{t}_2}}$ for $m_t = 170$ GeV.

we find that a neutrino signal from the centre of the Earth is beyond reach of the present and even future neutrino telescopes.

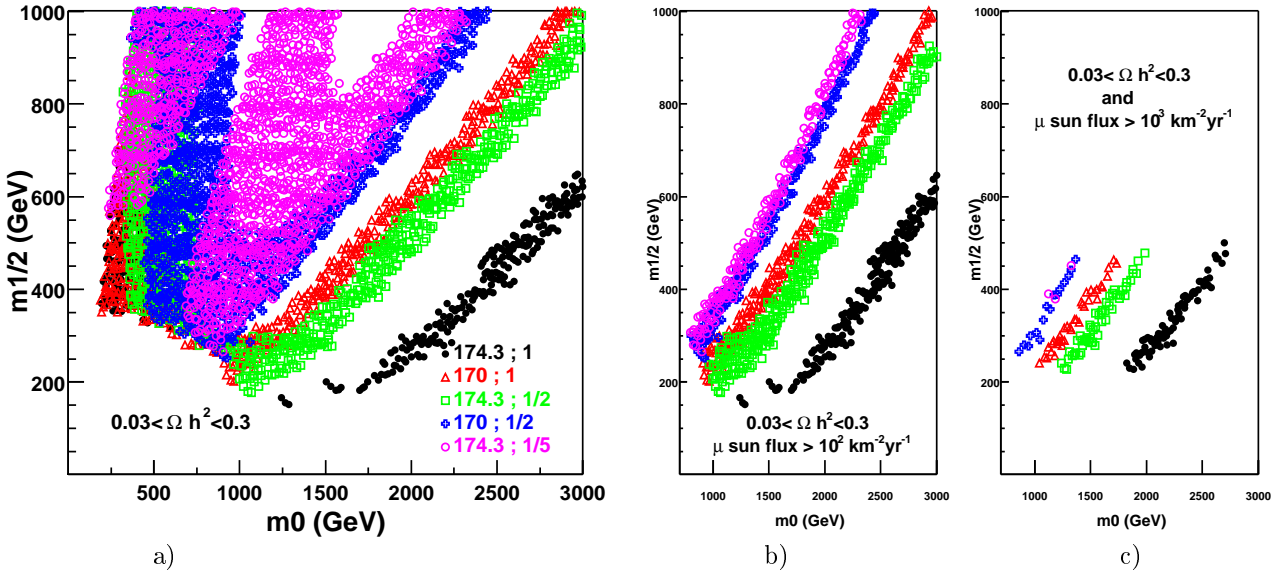


Figure 19: a) Dark matter favoured models for different values of Q_{EWSB} and top mass in the $(m_0, m_{1/2})$ plane (a). Colors and symbols correspond to different values of m_t and Q_{EWSB} : e.g. $(170 ; 1/2)$ means $m_t = 170$ GeV and $Q_{EWSB} = \frac{1}{2}\sqrt{m_{\tilde{t}_1}m_{\tilde{t}_2}}$. The models that moreover yield a muon flux from the Sun larger than $> 10^2 \text{ km}^{-2} \cdot \text{yr}^{-1}$ and $> 10^3 \text{ km}^{-2} \cdot \text{yr}^{-1}$ are shown in b) and c).

For the larger Sun, we find that a neutrino signal may be found, but only in the large m_0 "focus point" region [15, 28] where the neutralino has a larger higgsino component which increases both neutralino-nucleon elastic scattering and neutralino annihilation cross-sections. Since in this region, both are related by s - and t -channel crossing (exactly above $t\bar{t}$ threshold and approximately below), any parameter change reducing the relic density inevitably increases the neutrino flux. When conversion into muons is taken into account with a 5 GeV threshold on the muon energy, the only models providing both a relevant (but rather low) relic density, and fluxes around the *current* indirect detection sensitivity ($10^3 \mu \text{ km}^{-2} \cdot \text{yr}^{-1}$) are those with $m_\chi < m_t$ and $\chi\chi \xrightarrow{\chi_i^+} W^+W^-$ or $\chi\chi \xrightarrow{\chi_i} ZZ$ as dominant annihilation processes. Other kinds of models could favorize such channels to happen more generically [45]. The next generation of neutrino telescopes (with a km^3 size) will be much more efficient to probe mSugra models, especially for $m_\chi > m_t$. If a neutrino signal is found in this framework, then neutralino dark matter should also be accessible to future direct detection experiments, and a chargino with $m_{\chi^+} < 350$ GeV should be found in accelerators.

To conclude, a comparison with previous related work is in order. Earlier studies [8, 46] of neutralino indirect detection were performed in the unconstrained MSSM, where μ is a free parameter, and mixed neutralinos occur rather easily. Taking an mSugra slice in this huge parameter space obviously introduces many correlations, for instance between the neutrino flux and the relic density or $\sigma_{\chi-p}^{\text{spin}}$ (and even $\sigma_{\chi-p}^{\text{scal}}$). The effect of this slicing in the $(m_\chi, \sigma_{\chi-p}^{\text{scal}})$ plane was shown in [47] for small $\tan\beta$ and in [48] for large $\tan\beta$. Our fig. 9 agrees with this last result, with the addition of the focus point region forming the upper-right cloud. We should note however that a comparison in the $(m_0, m_{1/2})$ plane is more difficult, specially at large $\tan\beta$, because of the theoretical uncertainties in the RGE used to translate these parameters into physical quantities. As an example, for a given value of $\tan\beta$, the slope of the EWSB boundary decreases between [28], this work and [48]. As another example, the strong annihilation via s -channel A, H_0 scalars appears above $\tan\beta > 50$ in [49] and [50], $\tan\beta > 35$ in [48], and $\tan\beta > 60$ (or $\tan\beta = 45$, $Q_{EWSB} = \sqrt{m_{\tilde{t}_1}m_{\tilde{t}_2}}/5$, see fig. 16) in the present work using SUSPECT. Finally, we find a muon event rate compatible with [28], and larger than [49]. Part of this difference comes from a higher threshold (25 GeV instead of our 5 GeV). The rest might be attributed to a high sensitivity in the renormalization group equations at large m_0 and $\tan\beta$. It seems [24] that using SOFTSUSY [25] or SUSPECT [16, 17] may be safer than ISASUGRA[51] in this region.

Acknowledgements : This work would not have started without the french "GDR supersymetrie". We gratefully thank Jean-Loic Kneur, Charling Tao, and the Antares Neutralino WG for help and stimulating discussions.

References

- [1] J. A. Peacock. *Cosmological Physics*, chapter 3. Cambridge University Press, 1999.
- [2] C. H. Lineweaver. Cosmological parameters. 2001. talk presented at COSMO-01, Rovaniemi, Finland August 29 - September 4.
- [3] P. Fayet and S. Ferrara. Supersymmetry. *Phys. Rept.*, 32:249–334, 1977.
- [4] R. Barbieri. Looking beyond the standard model: The supersymmetric option. *Riv. Nuovo Cim.*, 11N4:1–45, 1988.
- [5] S. P. Martin. A supersymmetry primer. 1997.
- [6] J. A. Bagger. Weak-scale supersymmetry: Theory and practice. 1996.
- [7] H. E. Haber and G. L. Kane. The search for supersymmetry: Probing physics beyond the standard model. *Phys. Rept.*, 117:75, 1985.
- [8] G. Jungman, M. Kamionkowski, and K. Griest. Supersymmetric dark matter. *Phys. Rept.*, 267:195–373, 1996.
- [9] H. P. Nilles. Supersymmetry, supergravity and particle physics. *Phys. Rept.*, 110:1, 1984.
- [10] A. H. Chamseddine, R. Arnowitt, and P. Nath. Locally supersymmetric grand unification. *Phys. Rev. Lett.*, 49:970, 1982.
- [11] R. Barbieri, S. Ferrara, and C. A. Savoy. Gauge models with spontaneously broken local supersymmetry. *Phys. Lett.*, B119:343, 1982.
- [12] L. J. Hall, J. Lykken, and S. Weinberg. Supergravity as the messenger of supersymmetry breaking. *Phys. Rev.*, D27:2359–2378, 1983.
- [13] G. Gamberini, G. Ridolfi, and F. Zwirner. On radiative gauge symmetry breaking in the minimal supersymmetric model. *Nucl. Phys.*, B331:331–349, 1990.
- [14] J. L. Feng, K. T. Matchev, and T. Moroi. Focus points and naturalness in supersymmetry. *Phys. Rev.*, D61:075005, 2000.
- [15] J. L. Feng, K. T. Matchev, and F. Wilczek. Neutralino dark matter in focus point supersymmetry. *Phys. Lett.*, B482:388–399, 2000.
- [16] A. Djouadi, J.L. Kneur, and G. Moultaka. Suspect program, <http://www.lpm.univ-montp2.fr:7082/kneur/suspect.html>.
- [17] A. Djouadi, M. Drees, and J. L. Kneur. Constraints on the minimal supergravity model and prospects for susy particle production at future linear e+ e- colliders. *JHEP*, 08:055, 2001.
- [18] D. J. Castano, E. J. Piard, and Pierre Ramond. Renormalization group study of the standard model and its extensions. 2. the minimal supersymmetric standard model. *Phys. Rev.*, D49:4882–4901, 1994.
- [19] V. D. Barger, M. S. Berger, and P. Ohmann. The supersymmetric particle spectrum. *Phys. Rev.*, D49:4908–4930, 1994.
- [20] Damien M. Pierce, Jonathan A. Bagger, Konstantin T. Matchev, and Ren-jie Zhang. Precision corrections in the minimal supersymmetric standard model. *Nucl. Phys.*, B491:3–67, 1997.
- [21] P. Gondolo, J. Edsjo, L. Bergstrom, P. Ullio, and E. A. Baltz. Darksusy: A numerical package for dark matter calculations in the mssm. 2000.
- [22] P. Gondolo, J. Eds  , L. Bergstr  m, P. Ullio, and T. Baltz. Darksusy program, <http://www.physto.se/edsjo/darksusy/>.
- [23] T. Nihei, L. Roszkowski, and R. Ruiz de Austri. Towards an accurate calculation of the neutralino relic density. *JHEP*, 05:063, 2001.
- [24] B. C. Allanach. Theoretical uncertainties in sparticle mass predictions. 2001.
- [25] B. C. Allanach. Softsusy: A c++ program for calculating supersymmetric spectra. *Comput. Phys. Commun.*, 143:305–331, 2002.
- [26] D.E. et al Groom. Particle data group, <http://pdg.lbl.gov/>.
- [27] Marc Knecht and Andreas Nyffeler. Hadronic light-by-light corrections to the muon g-2: The pion-pole contribution. 2001.
- [28] J. L. Feng, K. T. Matchev, and F. Wilczek. Prospects for indirect detection of neutralino dark matter. *Phys. Rev.*, D63:045024, 2001.
- [29] S. Bertolini, F. Borzumati, A. Masiero, and G. Ridolfi. Effects of supergravity induced electroweak breaking on rare b decays and mixings. *Nucl. Phys.*, B353:591–649, 1991.

- [30] M. Ciuchini, G. Degrassi, P. Gambino, and G. F. Giudice. Next-to-leading qcd corrections to $b \rightarrow x/\gamma$: Standard model and two-higgs doublet model. *Nucl. Phys.*, B527:21–43, 1998.
- [31] R. Barate et al. Search for the neutral higgs bosons of the standard model and the mssm in $e^+ e^-$ collisions at $s^{**}(1/2) = 189$ -gev. *Eur. Phys. J.*, C17:223–240, 2000.
- [32] A. Heister et al. Final results of the searches for neutral higgs bosons in $e^+ e^-$ collisions at $s^{**}(1/2)$ up to 209-gev. *Phys. Lett.*, B526:191–205, 2002.
- [33] C. Boehm, A. Djouadi, and M. Drees. Light scalar top quarks and supersymmetric dark matter. *Phys. Rev.*, D62:035012, 2000.
- [34] J. R. Ellis, K. A. Olive, and Y. Santoso. Calculations of neutralino stop coannihilation in the cmssm. 2001.
- [35] R. Abusaidi et al. Exclusion limits on the wimp nucleon cross-section from the cryogenic dark matter search. *Phys. Rev. Lett.*, 84:5699–5703, 2000.
- [36] G. Chardin. Edelweiss dark matter search, talk given at the school and workshop on neutrino particle astrophysics, les houches 21 jan -1rst feb. 2002.
- [37] N. Spooner. New limits and progress from the boulby dark matter programme, talk given at the school and workshop on neutrino particle astrophysics, les houches 21 jan -1rst feb. 2002.
- [38] F. Mayet, D. Santos, Yu. M. Bunkov, E. Collin, and H. Godfrin. Search for supersymmetric dark matter with superfluid he-3 (mache3). 2002.
- [39] Olga V. Suvorova. Status and perspectives of indirect search for dark matter. 1999.
- [40] T. Montaruli. Proceedings of icrc1999.
- [41] A. Habig. Proceedings of icrc2001.
- [42] L. Thompson. Dark matter prospects with the antares neutrino telescope, talk given at the conference dark 2002, cape town, south africa 4-9 feb. 2002.
- [43] J. Edsjo. Swedish astroparticle physics, talk given at the conference partikeldagarna, uppsala, sweden, march 6. 2001.
- [44] J. R. Ellis, T. Falk, K. A. Olive, and M. Srednicki. Calculations of neutralino stau coannihilation channels and the cosmologically relevant region of mssm parameter space. *Astropart. Phys.*, 13:181–213, 2000.
- [45] E. Nezri. in preparation.
- [46] Lars Bergstrom, Joakim Edsjo, and Paolo Gondolo. Indirect detection of dark matter in km-size neutrino telescopes. *Phys. Rev.*, D58:103519, 1998.
- [47] John R. Ellis, Andrew Ferstl, and Keith A. Olive. Re-evaluation of the elastic scattering of supersymmetric dark matter. *Phys. Lett.*, B481:304–314, 2000.
- [48] John R. Ellis, Andrew Ferstl, and Keith A. Olive. Constraints from accelerator experiments on the elastic scattering of cmssm dark matter. 2001.
- [49] Vernon D. Barger, Francis Halzen, Dan Hooper, and Chung Kao. Indirect search for neutralino dark matter with high energy neutrinos. *Phys. Rev.*, D65:075022, 2002.
- [50] L. Roszkowski, R. Ruiz de Austri, and T. Nihei. New cosmological and experimental constraints on the cmssm. *JHEP*, 08:024, 2001.
- [51] Howard Baer, Frank E. Paige, Serban D. Protopopescu, and Xerxes Tata. Isajet 7.48: A monte carlo event generator for $p p$, anti- $p p$, and $e^+ e^-$ reactions. 1999.